INSTITUTE OF PHYSICS PUBLISHING JOURNAL OF PHYSICS D: APPLIED PHYSICS

J. Phys. D: Appl. Phys. **39** (2006) 3932–3938 doi:10.1088/0022-3727/39/18/002

Eddy current damping for magnetic levitation: downscaling from macro- to micro-levitation

C Elbuken, M B Khamesee[1] and M Yavuz

Department of Mechanical and Mechatronics Engineering, University of Waterloo, Ontario, Canada

E-mail: celbuken@uwaterloo.ca, khamesee@uwaterloo.ca and myavuz@uwaterloo.ca

Received 25 May 2006, in final form 18 July 2006
Published 1 September 2006
Online at stacks.iop.org/JPhysD/39/3932

Abstract

Magnetic levitation of miniaturized objects is investigated in this paper. A magnetic levitation setup is built to implement one-dimensional magnetic levitation motion. It was observed that as the levitated object becomes smaller, magnetic levitation suffers more from undesired vibrations. As a solution, eddy current damping is offered and implemented successfully by placing conductive plates close to the levitated object. An analytical expression for damping coefficient is derived. Experimentally, it is shown that eddy current damping can reduce the RMS positioning error to the level of more than one third of its original value for a 0.386 g object levitated in an air-gap region of 290 mm. The proposed system has the potential to be used for micro-manipulation purposes in a high motion range of 39.8 mm.

1. Introduction

There has been a great deal of research on micro-manipulation and micro-positioning using magnetic principles. Magnetic levitation is a promising technology which can be applied for such applications, since it does not use long-reached and jointed parts. Therefore, wear and maintenance problems caused by friction are completely eliminated. Magnetic levitation has uses in teleoperation [1–3], micro-positioning stages [4–7], magnetic bearings [8, 9] and micro-electronic fabrication [10–12]. Although, magnetic levitation systems realized up to now can achieve micro-accuracy, the levitated structures are in macro scale.

In 2002, Morita *et al* [13] introduced a micro-levitation system that levitates a small iron ball of 2 mm in a range of 40 μm. The system balances the weight of the ball by utilizing motion control of the levitation unit which carries a permanent magnet. The distance between the levitated object and the assembled permanent magnet is controlled to equate the attractive force to the weight of the levitating object. Although magnetic levitation of the ball in one degree of freedom (1-DOF) is achieved, experimental results indicate that the ball experienced high vibrations. Also, the motion range of this setup is limited with the stroke of the piezoelectric actuator which is on the order of microns.

In this work, we propose using a macroscopic magnetic drive unit for high-precision levitation of micro-objects. The system allows positioning of an object in a large air-gap by controlling the magnetic field generated by electromagnets. The motivation behind this study is that, due to non-contact manipulation, magnetic levitation eliminates friction and adhesion forces which are the two dominant forces in micro-scale. In addition, since the power required for motion is generated by the magnetic drive unit, the levitated device itself does not require to carry any power source or controller. This allows reducing the dimensions and complexity of the levitated object. Therefore, it is possible to realize a levitating micro-electro-mechanical system (MEMS) that can achieve numerous tasks using the proposed technology. Since such a device has the ability to combine sensing, processing and actuation on a single structure, it can be applicable to micro-assembly and micro-manipulation tasks in hazardous environments and portable clean room applications.

Towards the goal of micro-levitation, magnetic levitation experiments of mm-sized NdFeB (Neodymium Iron Boron) permanent magnets are presented. Similar to Morita's results

[1] Author to whom any correspondence should be addressed.

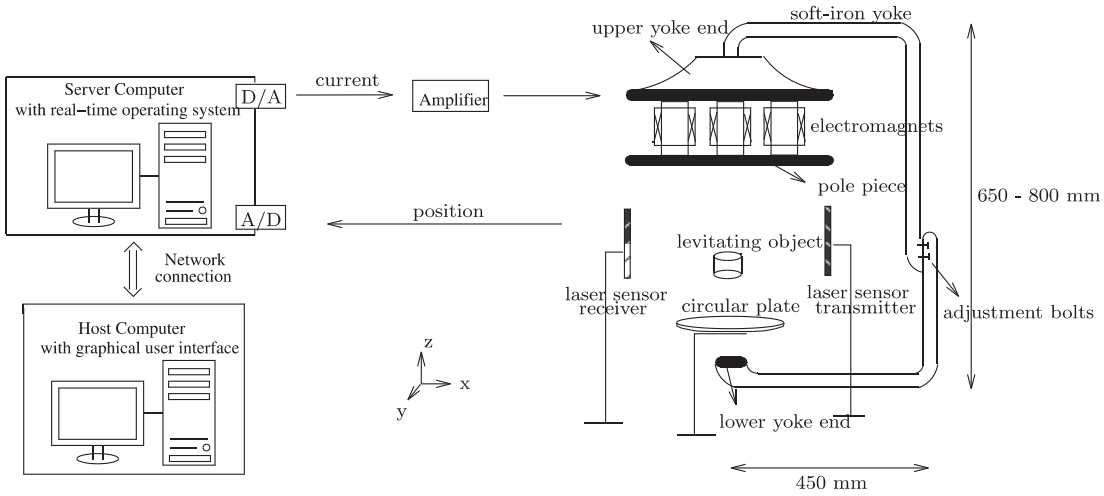

Figure 1. Schematic of magnetic levitation system.

[13], it was observed that magnetic levitation suffers from high vibrations due to contactless motion and low environment stiffness. In addition, it was observed that undesired vibrations increase for magnetic levitation as the object size gets smaller. Therefore, vibration is a big challenge to overcome for micro-levitation studies.

Teshima *et al* [14] suggested eddy current damping (magnetic damping) in order to damp vibrations in a superconducting levitation system; however, the discussion was mostly based on experimental work. A damping coefficient was determined from the experimental measurement of dynamic stiffness of the system. In fact, eddy current damping is the optimum way of adding extra damping to levitation systems because of its non-contact nature. Moreover, eddy current damping does not affect the controller algorithm or the complexity of the system and does not degrade over time [15].

Although the studies related to eddy currents go back to Maxwell [16], the problem of eddy currents in bounded conductors was first discussed by Jeans using the image method [17]. Smythe [18] solved the same problem in a more practical way and his results were used by Davis and Reitz [20] to explain the eddy currents in bounded conductors and to calculate the forces applied by the eddy currents to a magnet nearby. Saslow [19] provided a fine explanation of Maxwell's eddy current theory as well as some examples of the effects of eddy current and an overlook to Jeans's studies. Various studies followed these pioneers that discuss braking and damping effects of eddy currents [21–24]. In this study, eddy current damping is employed for a magnetic levitation system to improve the levitation precision of miniaturized objects and a damping coefficient is derived to quantify the damping effect.

This paper is organized as follows. Section 2 explains the magnetic levitation system and the controller algorithm. Experimental results of levitation of various permanent magnets are presented in section 3. In section 4, eddy current damping is introduced to the system and derivation of a damping coefficient is described. In section 5, the performance of the proposed damping mechanism is evaluated based on the levitation experiments.

2. Magnetic levitation system

The schematic of the magnetic levitation system is shown in figure 1. The set-up consists of a controller, a CCD laser line displacement sensor, an iron yoke and seven electromagnets connected with a pole piece. Since the vertical motion of the object is examined, the laser sensor measures the $\hat{z}$-axis position only. The 0.2–40 mm measuring range of the laser sensor results in a motion range of 39.8 mm for the levitated object. The position feedback is provided at every 5 ms. The real-time controller communicates to the system through 16-bit A/D and 16-bit D/A converters with operating ranges of ± 5 V and ± 10 V, respectively. A host computer with a graphical user interface is used to gain access to the system.

The levitation system uses a proportional derivative closed-loop controller. The position of the levitated object is continuously detected by the laser sensor and sampled by the A/D converter. Based on the position data, the velocity of the object is calculated by a difference equation. Multiplying the position and the velocity with controller gains, the current that needs to be applied to the electromagnets is determined. Since the same current is applied to all electromagnets, the object moves along the central axis of the air-gap. The controller is designed by a state feedback controller design approach. For 1-DOF levitation, the governing equation of motion can be written as

$$m\frac{\mathrm{d}^2 z}{\mathrm{d}t^2} = F_{\mathrm{lev}} - mg, \tag{1}$$

where m is the mass of the levitated object, g is the gravitational acceleration and F_{lev} is the $\hat{z}$ component of the levitation force applied by the magnetic drive unit. For a permanent magnet that has a net dipole moment of p_0 in $\hat{z}$ direction, the vertical levitation force can be expressed as [25]

$$F_{\mathrm{lev}} = p_0 \frac{\partial B_z}{\partial z}, \tag{2}$$

where B_z is the vertical magnetic flux density generated by the levitation system. Due to the effect of yoke and pole piece, obtaining a formula for magnetic flux density is very

Figure 2. Picture of the levitation system.

challenging. Therefore, in a previous study of the authors, an experimental method was followed to derive a formula for the levitation force to be [26]

$$F_{\text{lev}} = \alpha I z + \beta I, \tag{3}$$

where α and β are fitting constants, I is the current applied to the electromagnets and z is the distance between the object and the pole piece. Substituting equation (3) into (1), the differential equation of the system is derived as

$$m\frac{\mathrm{d}^2 z}{\mathrm{d}t^2} = \alpha I z + \beta I - mg. \tag{4}$$

The state variables are chosen as position ($z = x_1$) and velocity ($(\mathrm{d}z/\mathrm{d}t) = x_2$) of the levitating object. Defining the input of the system as the current (I) applied to the electromagnets, state equations of the system can be obtained as shown below

$$\frac{\mathrm{d}x_1}{\mathrm{d}t} = x_2, \tag{5}$$

$$\frac{\mathrm{d}x_2}{\mathrm{d}t} = \frac{\alpha}{m} I x_1 + \frac{\beta}{m} I - g. \tag{6}$$

By linearizing the system around multiple working points (I_0, z_0) using Lagrange's method, the state matrices can be found as

$$X = \begin{bmatrix} x_1 \\ x_2 \end{bmatrix}, \qquad U = I, \qquad \frac{\mathrm{d}X}{\mathrm{d}t} = AX + BU, \tag{7}$$

$$A = \begin{bmatrix} 0 & 1 \\ \frac{\alpha}{m} I_0 & 0 \end{bmatrix}, \qquad B = \begin{bmatrix} 0 \\ \frac{\alpha}{m} z_0 + \frac{\beta}{m} \end{bmatrix}. \tag{8}$$

Using a proportional derivative control strategy, the current can be determined by

$$I = I_0 - [K_1(x_1 - z_0) + K_2 x_2], \tag{9}$$

where K_1 and K_2 are the feedback gains determined by pole placement.

3. Levitation of NdFeB magnets

To test the capability of the system for levitation of small magnets, various permanent magnets were levitated. The picture of the experimental set-up is shown in figure 2. The experiments were carried out with different sizes of cylindrical NdFeB magnets. The weights and the dimensions of the magnets are summarized in table 1. Step inputs were applied to the system as reference for the levitated object to follow (shown as dashed lines in figure 3). For each magnet, feedback gains were recalculated (K_1, K_2) and fine-tuned experimentally to obtain the best possible performance.

Table 1. Magnet properties and experimental RMS position error.

	(a)	(b)	(c)	(d)
Magnet weight (mg)	5950	757	386	140
Radius (mm) × thickness (mm)	5 × 10	2.5 × 5	2.5 × 2.5	2 × 1.5
RMS error for $z = -0.084$ m (μm)	22.58	32.75	55.90	50.42
RMS error for $z = -0.083$ m (μm)	19.07	43.55	78.25	134.77
Average RMS error (μm)	20.83	38.15	67.08	92.60

The experimental results are illustrated in figure 3. It is observed that when the levitated object size is decreased, less precision is obtained. The RMS position errors for each experiment are calculated (table 1)[1]. The overshoot due to the step input and noise cause smaller objects to experience higher vibrations around the reference position. The average position error is 20.83 μm for the largest magnet while it is 92.60 μm for the smallest one. Therefore, the levitation of small objects suffers from the low environment stiffness and requires a damping mechanism.

The drastic increase in the positioning error for small objects might be because of the increasing effect of noise on a smaller object. Due to the scaling laws, the electrostatic force becomes dominant in micro-scale, while gravitational force loses significance. Therefore, electrostatic noise in the environment is more effective on a smaller object. Also, any inherent noise in the system, which can be caused by measurement noise and conversion errors is more disturbing for a smaller object. In addition, air drag force which is neglected in the dynamic equation of motion in the controller design is more significant for a smaller object. The air drag force is scaled down by two (proportional to surface area) while the mass of the system is scaled by three (proportional to volume) resulting in a larger acceleration due to $a = F/m$. All these factors contribute to the larger deflection in the positioning of small objects.

4. Eddy current damping

Because of non-contact motion and low environment stiffness, an additional mechanism is required to suppress the oscillations of the levitated object. The authors propose an eddy current damping mechanism (magnetic damping) to improve the precision of motion because of its ease of employment and contactless operation. In addition, eddy current damping does not require a change in the controller algorithm or does not increase the cost or complexity of the system. In this section, a quantitative analysis of magnetic damping is presented that forms the guidelines of optimum eddy current damper design for magnetic levitation systems.

[1] RMS error is calculated starting from the second crossing of the position data with the reference input, so the first overshoot is not taken into account.

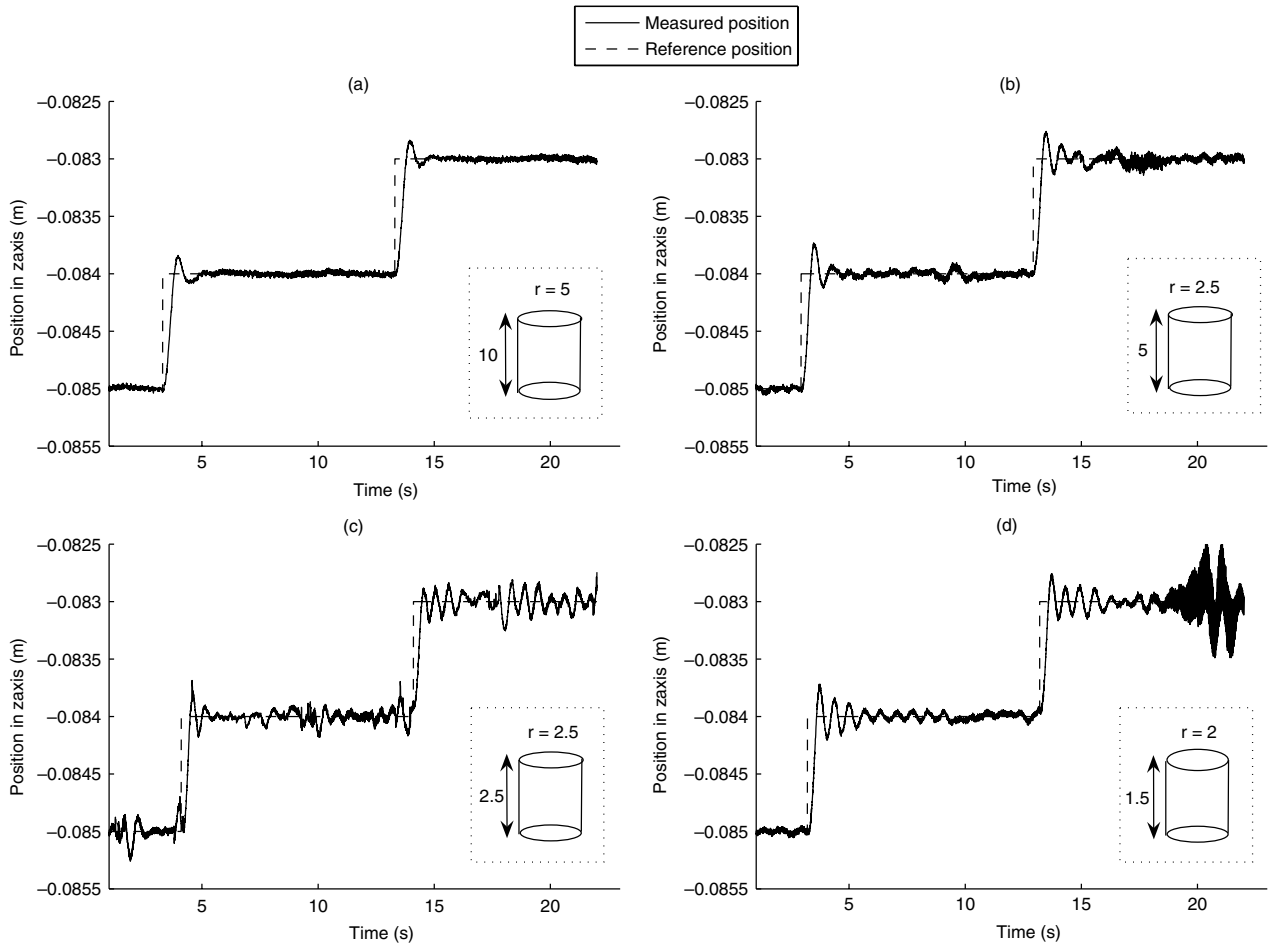

Figure 3. Step responses of cylindrical objects with different dimensions (radius × thickness): (*a*) 5 mm × 10 mm, (*b*) 2.5 mm × 5 mm, (*c*) 2.5 mm × 2.5 mm, (*d*) 2 mm × 1.5 mm.

Eddy current damping can be introduced to the system by placing non-ferromagnetic (aluminium, copper, bronze, brass, etc) plates underneath the levitated object. Since levitated objects are cylindrical, disc-shaped plates are used that simplifies the analytical calculation of flux passing through the plate to a great extent. The 6061-Al disc is placed on a glass stand, below the working domain of the magnet (figure 1).

During the oscillations of the levitated object, a changing magnetic field is generated in the air-gap region. The time-varying magnetic field has two sources: (1) The change in the field generated by the electromagnets (when the position of the object changes, the controller adjusts the currents supplied to the electromagnets); (2) The self-magnetic field of the moving permanent magnet. If a conductor is placed in the varying field, circulating eddy currents are formed. The direction of the current is such that magnetic field generated by this eddy current opposes the change in the field itself. Consequently, the conductor serves as a damper to the levitating magnet.

The experimental results presented in section 3 reveals that small objects have an oscillatory motion of levitation. Therefore, the magnetic flux in the vicinity of the object oscillates, as well.

In order to calculate the damping coefficient, flux penetrating the Al-disc should be determined. The magnetic flux has two components: Φ_{em} and Φ_{pm} that are the fluxes generated by the electromagnets and the permanent magnet, respectively. Although Φ_{pm} can easily be calculated, calculation of Φ_{em} is quite complicated because of the effect of the pole piece that connects the electromagnets. Therefore, oscillatory motion of the object is approximated by a sine function as illustrated in figure 4. For simplicity, flux penetrating the disc can be expressed as

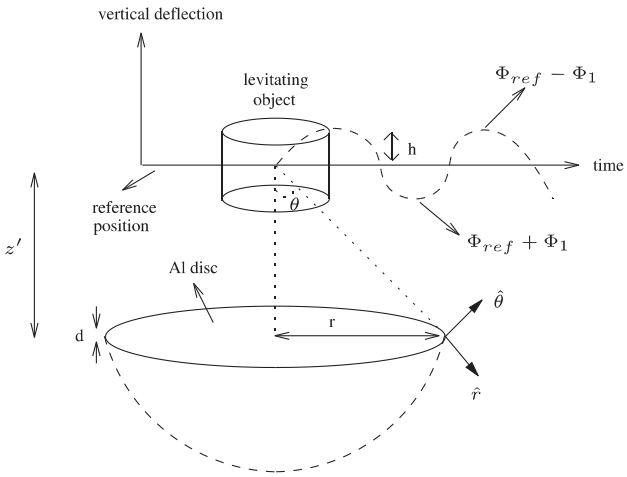

Figure 4. Oscillatory motion of the permanent magnet above the circular plate.

$$\Phi(t) = \Phi_{\text{ref}} - \Phi_1 \sin(2\pi f t), \tag{10}$$

where Φ_{ref} is the flux penetrating the disc when the magnet is at reference position and f is the frequency of oscillation. Therefore, the flux penetration when the magnet moves to the lower peak position becomes $\Phi_{ref} + \Phi_1$ (figure 4). Then Φ_1 can be written as

$$\Phi_1 = \Phi_{peak} - \Phi_{ref}, \tag{11}$$

where Φ_{peak} is the flux penetration for the magnet's lower peak position. The flux penetration through the plate due to the permanent magnet can easily be calculated when a circular plate is used. In spherical coordinates, magnetic flux density of the permanent magnet can be written as [27]

$$\boldsymbol{B} = \frac{\mu_0}{4\pi} p_0 \left(\hat{r} \frac{2\cos\theta}{r^3} + \hat{\theta} \frac{\sin\theta}{r^3} \right), \tag{12}$$

where p_0 is the dipole moment of the magnet and θ is the angle from the central axis. Flux passing through the plate is equal to the flux passing through the outer surface of the semi-sphere shown as the dashed line in figure 4. Then penetrating flux can be found as

$$\begin{aligned} \Phi_{pm} &= \int \boldsymbol{B} \cdot \mathrm{d}\boldsymbol{s} = \int_{sph} \boldsymbol{B} \cdot \hat{r} \mathrm{d}s \\ &= \int_0^{\cos^{-1} \frac{z'}{\sqrt{z'^2+r^2}}} \int_0^{2\pi} B_r r^2 \sin\theta \, \mathrm{d}\phi \mathrm{d}\theta \\ &= \frac{\mu_0}{2} p_0 \frac{r^2}{(r^2 + z'^2)^{3/2}}, \end{aligned} \tag{13}$$

where z' is the object-disc distance and r is the radius of the disc.

Equation (11) can be decomposed into components from the permanent magnet (pm) and the electromagnets (em):

$$\Phi_1 = (\Phi_{pm,peak} + \Phi_{em,peak}) - (\Phi_{pm,ref} + \Phi_{em,ref}). \tag{14}$$

Then, using equation (13), Φ_{peak} and Φ_{ref} take the following forms:

$$\Phi_{peak} = \frac{\mu_0}{2} p_0 \frac{r^2}{(r^2 + (z' - h)^2)^{3/2}} + \Phi_{em,peak}, \tag{15}$$

$$\Phi_{ref} = \frac{\mu_0}{2} p_0 \frac{r^2}{(r^2 + z'^2)^{3/2}} + \Phi_{em,ref}. \tag{16}$$

Substituting equations (15) and (16) into (14), the analytical expression for Φ_1 can be obtained as

$$\Phi_1 = \frac{\mu_0}{2} p_0 \left[\frac{r^2}{(r^2 + (z' - h)^2)^{3/2}} - \frac{r^2}{(r^2 + z'^2)^{3/2}} \right] + \Delta\Phi_{em}. \tag{17}$$

Obtaining an expression for Φ_1 suffices to derive a damping coefficient since the Φ_0 component in equation (10) does not have a time dependence and does not contribute to the varying magnetic field.

Representing the conducting disc as N turns of wire and using equation (10), the induced electromotive force in the conductor can easily be found as

$$V_{ind} = -N \frac{\mathrm{d}\Phi}{\mathrm{d}t} = N 2\pi f \Phi_1 \cos(2\pi f t). \tag{18}$$

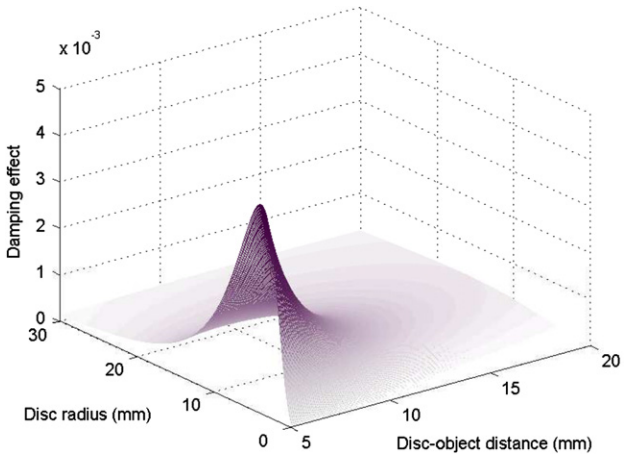

Figure 5. The effect of disc radius and disc–object distance on damping coefficient. $h = 0.2$ mm.
(This figure is in colour only in the electronic version)

Then the average power dissipation in the conductor can be calculated as

$$P_{avg} = \frac{1}{T} \int_{t_0}^{t_0+T} \frac{V_{ind}^2}{R} \mathrm{d}t = \frac{(N 2\pi f \Phi_1)^2}{2R}, \tag{19}$$

where $T = 1/f$ is the period of the motion and R is the resistance of the path that eddy currents travel.

Denoting the force causing the vibrations as F and assuming that the magnet moves with an average speed of v during oscillations, the power dissipation can be written as

$$P_{avg} = F v. \tag{20}$$

The frequency of vibration is found as $f = v/(2h)$ using the maximum deflection during oscillation which is denoted as h in figure 4. Then equation (19) takes the form

$$P_{avg} = \frac{(N 2\pi \Phi_1)^2}{2R} \cdot \left(\frac{v}{2h} \right)^2 = \frac{(N\pi \Phi_1 v)^2}{2Rh^2}. \tag{21}$$

Substituting equation (21) into (20) yields

$$F = \frac{(N\pi \Phi_1)^2}{2Rh^2} v. \tag{22}$$

Using the relationship between the force and velocity, $F = cv$, it is now possible to write the damping coefficient as follows:

$$c = \frac{(N\pi \Phi_1)^2}{2Rh^2}. \tag{23}$$

To investigate the optimum damping, this damping coefficient should be expressed as a function of plate parameters. For that purpose N can be written as

$$N = \frac{dr}{a}, \tag{24}$$

where d is the disc thickness, r is the disc radius and a is the cross-sectional area of the current pathway. The resistance of the path of current can be calculated by

$$R = \frac{l}{\sigma a}, \tag{25}$$

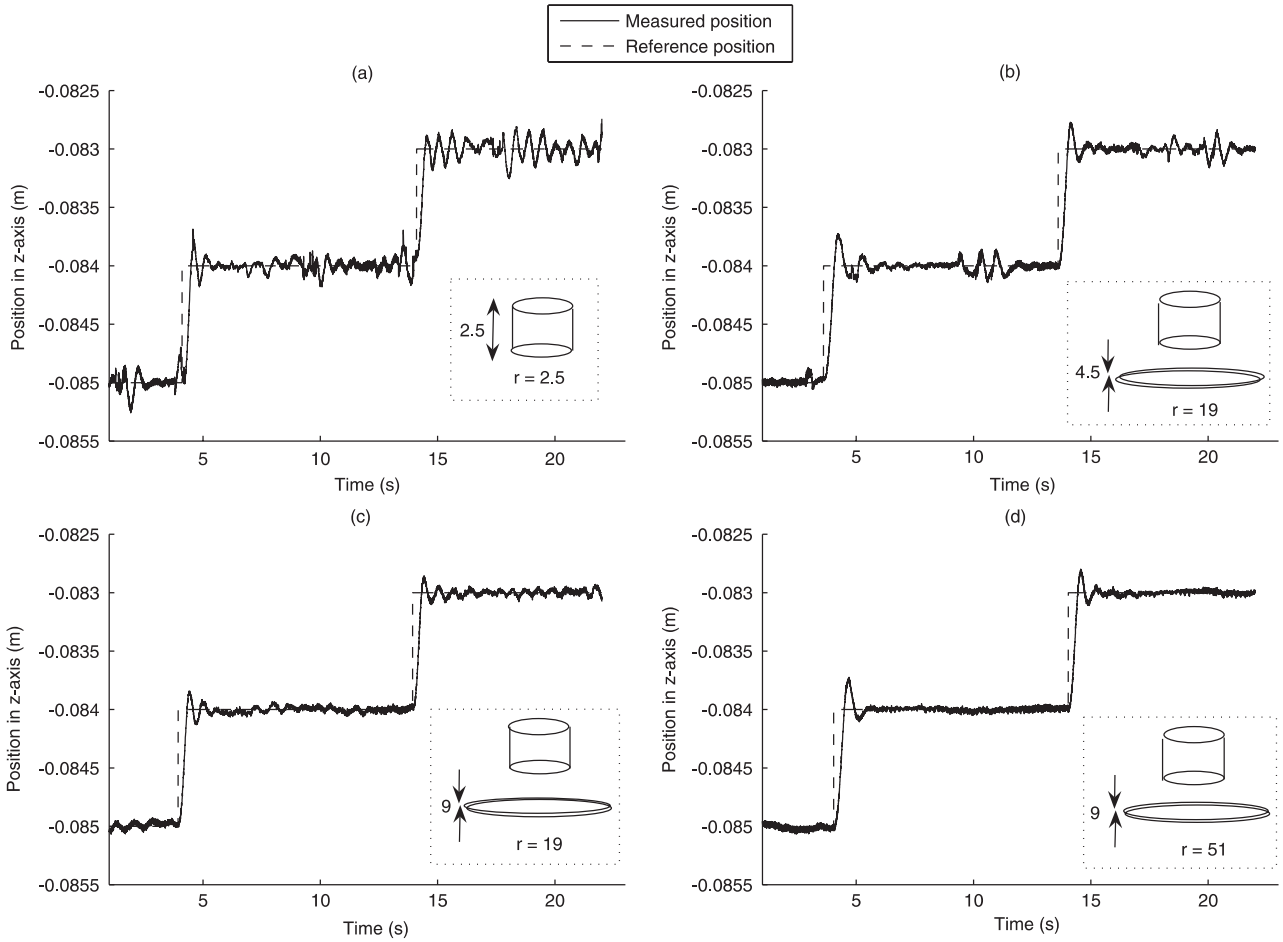

Figure 6. Step responses of 2.5 mm × 2.5 mm magnet with/without eddy current dampers: (*a*) no damper, (*b*) 19 mm × 4.5 mm disc, (*c*) 19 mm × 9 mm disc, (*d*) 51 mm × 9 mm disc.

where $l = N2\pi\frac{r}{2} = N\pi r$. Substituting equation (25) into (23), the damping coefficient can be found as

$$c = \frac{d\pi\sigma\Phi_1^2}{2h^2}. \tag{26}$$

Equation (26) indicates that damping introduced by the disc is proportional to the disc thickness and conductivity. However, it should be emphasized that eddy currents penetrate up to a certain depth from the surface of the disc, which is given by the penetration depth. Therefore, it is expected to observe a saturation of the damping, if the disc thickness is increased further than the standard penetration depth.

The other two parameters that affect the damping coefficient are the disc radius (r) and disc-object distance (z') which are the variables that change Φ_1 in equation (26). Intuitively, disc radius (r) should have a similar effect on damping as the disc thickness (d), i.e. increasing disc radius should increase the damping. However, when the disc is placed close to the magnet, a larger disc will cut through more returning flux (flux with a positive $\hat{z}$ component) and there will be a decrease in the net flux penetrating the disc, resulting in a smaller damping.

The relationship between the damping coefficient and the disc radius can be investigated by using equation (17). Figure 5 illustrates the term in square brackets in equation (17), plotted for a certain deflection from the reference position (h). $\Delta\Phi_{em}$ is not included, since there is not an analytical expression for the magnetic field generated by the magnetic drive unit that consists of electromagnets, pole piece and a returning yoke. However, due to the effect of the returning yoke, electromagnets generate a uniform magnetic field in the motion range of interest. Therefore, $\Delta\Phi_{em}$ has a linear effect on the plot in figure 5, which would simply shift the curve up for increasing disc radius without affecting the observed behaviour. The plot indicates that up to a certain limit, increasing disc radius increases the damping effect. Although a further increase in radius increases the $\Delta\Phi_{em}$ term in equation (17), the change in damping will not be as significant because of the decrease observed in the plot. The critical radius for which damping is maximized (around 10 mm in figure 5), is a function of maximum deflection (h) and disc-object distance (z'). Therefore, to maximize the damping effect, damper dimensions and location should be set using equation (17).

5. Levitation of NdFeB magnets with damping

The proposed mechanism was applied to the levitation of the magnet with 2.5 mm radius and 2.5 mm height. In section 3, it was demonstrated that this magnet experiences large vibrations

Table 2. Disc dimensions and RMS position error with damping.

	(a)	(b)	(c)
Plate radius (mm) × thickness (mm)	19 × 4.5	19 × 9	51 × 9
RMS error for $z = -0.084$ m (μm)	42.69	22.10	20.16
RMS error for $z = -0.083$ m (μm)	45.89	22.72	20.44
Average RMS error (μm)	44.29	22.41	20.30

during levitation. To observe the effect of eddy current, levitation of the same magnet was carried out with eddy current damping in this section. Three Al-6061 discs were prepared with different radii and thicknesses as specified in table 2. The same reference input was given to the system while the discs were placed as dampers. For all experiments, the discs were kept at $z = -0.090$ m which resulted in a maximum disc-object distance of 7 mm.

For comparison, the experimental results without damping and with different dampers are illustrated in figure 6. The experiments confirm that eddy current damping is very effective in suppressing vibrations. Even the smallest disc (19 mm × 4.5 mm) improved the levitation performance significantly (figure 6(*b*)). It was observed that as the disc thickness increased, higher precision was achieved (figure 6(*c*)). In addition, as equation (17) implies, increasing the disc radius from 19 to 51 mm did not result in a significant change in precision. The RMS error decreased from 22.41 to 20.30 μm (figures 6(*c*) and (*d*)) due to the behaviour plotted in figure 5.

Using a two-step input allowed one to observe the effect of disc-object distance on damping, as well. The disc was located at $z = -0.090$ m. When the object was levitated from -0.084 to -0.083 m, the disc distance increased from 6 to 7 mm. The RMS position errors for each height were calculated separately. Although, it is hard to observe the difference with the naked eye, table 2 indicates the slight increase in error for $z = -0.083$ m compared with $z = -0.084$ m. Therefore, the damping effect decreases and larger vibrations are observed when disc-object distance increases as illustrated in figure 5.

6. Conclusion

In this paper, the issues of downscaling in magnetic levitation—particularly damping of oscillations is discussed. Levitation of tiny magnets of various sizes was demonstrated towards the goal of micro-levitation. It is observed that when the size of the levitated object decreases, less precision is achieved. Eddy current damping was proposed to improve the performance of levitation of miniaturized objects without a need to change the controller algorithm. Aluminium discs were placed underneath the levitated object to generate the eddy currents. To quantify the damping effect, a damping coefficient was derived by modelling the disc as multiple turns of coil. It was shown that damping can be optimized by varying the radius, thickness, conductivity of the disc and the distance between the disc and levitating object. The experiments with the damping mechanism verified that excessive energy that causes vibrations is dissipated as eddy currents in the disc. The proposed system has the capability of levitating a 2.5 mm × 2.5 mm magnet in a motion range of 39.8 mm in a 290 mm air-gap. As future work, a 3D controller algorithm will be developed that will realize a system for potential applications in micro-positioning and micro-manipulation.

References

[1] Lin C E and Jou H L 1997 *Proc. Nat. Sci. Counc., Rep. China* A **21** 222
[2] Salcudean S E, Wong N M and Hollis R L 1995 *IEEE J. Robot. Automat.* **11** 844-58
[3] Koumboulis F N and Skarpetis M G 1996 *IEE Proc. Control Theory Appl.* **143** 338
[4] Verma S, Kim W J and Gu J 2004 *IEEE/ASME Trans. Mechatron.* **9** 384–91
[5] Jung K S and Baek Y S 2002 *IEEE/ASME Trans. Mechatron.* **7** 35-43
[6] Shan X, Kuo S K, Zhang J and Menq C H 2002 *IEEE/ASME Trans. Mechatron.* **7** 67–78
[7] Kim W J and Trumper D L 1998 *Precision Eng.* **22** 66–77
[8] Komori M and Shiraishi C 2003 *IEEE Trans. Appl. Supercond.* **13** 2189–92
[9] Mukhopadhyay S C, Donaldson J, Sengupta G, Yamada S, Chakraborty C and Kacprzak D 2003 *IEEE Trans. Magn.* **39** 3220–2
[10] Park K H, Ahn K Y, Kim S H and Kwak Y K 1998 *IEEE/ASME Trans. Mechatron.* **3** 73–8
[11] Motokawa M, Hamai M, Sato T, Mogi I, Awaji S, Watanabe K, Kitamura N and Makihara M 2001 *J. Magn. Magn. Mater.* **226–300** 2090–3
[12] Holmes M, Hocken R and Trumper D 2000 *J. Int. Soc. Precision Eng. Nanotechnol.***24** 191–209
[13] Morita T, Shimizu K, Hasegawa M, Oka K and Higuchi T 2002 *IEEE Trans. Contr. Syst. Technol.* **10** 666–70
[14] Teshima H, Tanaka M, Miyamoto K, Noghuchi K and Hinata K 1997 *Physica* C **274** 17–23
[15] Sodano H A and Bae J S 2004 *Shock Vib. Digest* **36** 469–78
[16] Maxwell J C 1872 *Proc. R. Soc. Lond.* **20** 160–8
[17] Jeans J H 1899 *Proc. Math. Soc. Lond.* **31** 151–69
[18] Smythe W R 1942 *Trans. Am. Inst. Electr. Eng.* **61** 681–4
[19] Saslow W M 1992 *Am. J. Phys.* **60** 693–711
[20] Davis L C and Reitz J R 1971 *J Appl. Phys.* **42** 4119–27
[21] Wiederick H D, Gauthier N, Campbell D A and Rochon P 1987 *Am. J. Phys.* **55** 500–3
[22] Heald M A 1988 *Am. J. Phys.* **56** 521–2
[23] Marcuso M, Gass R, Jones D and Rowlett C 1991 *Am. J. Phys.* **59** 1123–9
[24] Aguiregabiria J M, Hernandez A and Rivas M 1997 *Am. J. Phys.* **65** 851–6
[25] Khamesee M B, Kato N, Nomura Y and Nakamura T 2002 *IEEE/ASME Trans. Mechatron.* **7** 1–14
[26] Shameli E, Khamesee M B and Huissoon J P 2006 *Proc. ASME/JSME Conf. on Micromechatronics for Information and Precision Equipment (Santa Clara, USA)*
[27] Inan U S and Inan A S 1999 *Engineering Electromagnetics* (Menlo Park, CA: Addison-Wesley) p 502